

Original Research Article

The reinfection threshold, revisited

F.M.G. Magpantay^{a,*}, J. Mao^{a,b}, S. Ren^a, S. Zhao^a, T. Meadows^a^a Department of Mathematics and Statistics, Queen's University, 48 University Avenue, Kingston, ON, Canada, K7L 3N6^b Department of Physics, Engineering Physics and Astronomy, Queen's University, 64 Bader Lane, Kingston, ON, Canada, K7L 3N6

ARTICLE INFO

Keywords:

Leaky immunity
Mathematical epidemiology

ABSTRACT

One mode by which infection-derived immunity fails is when recovery leads to a reduced but nonzero risk of reinfection. This type of partial protection is called leaky immunity with the degree of leakiness quantified by the relative probability a previously infected individual will get infected upon exposure compared to a naively susceptible individual. Previous authors have defined the reinfection threshold, which occurs when the basic reproduction number equals the inverse of the leakiness, however, there has been some debate about whether or not this is a real threshold. Here we show how the reinfection threshold relates to two important occurrences: (1) the point at which the endemic equilibrium changes from being a stable spiral to a stable node, and (2) the point at which the rate of change of the prevalence increases the most relative to leakiness. When the recovery period is short relative to the average lifetime then both occurrences are close to the reinfection threshold. We show how these results are related to the reinfection threshold found in other models of imperfect immunity. To further demonstrate the significance of this threshold in modeling, we conducted a simulation study to evaluate some of the consequences the reinfection threshold might have in parameter estimation and modeling. Using specific parameter values chosen to reflect an acute infection, we found that the basic reproduction number values larger than that of the reinfection threshold value were less identifiable than those below the threshold.

1. Introduction

The emergence and reemergence of infectious diseases such as Zika, COVID-19, monkeypox, and polio has led to growing interest in the different types of natural immunity that develop following an infection. For some diseases like measles [1] and smallpox [2], infection-derived immunity is assumed to be perfect and lifelong, allowing the dynamics to be modeled using the classical Susceptible–Infectious–Recovered/Removed (SIR) model. For other diseases like gonorrhea and meningitis [3], immunity is assumed to be nonexistent, and these systems can be modeled using the Susceptible–Infectious–Susceptible (SIS) model. Between the SIR and SIS models are many different modes by which natural immunity can provide imperfect protection, with each mode having a continuum of degrees of protectiveness [4]. Here we take a closer look at leaky partial protection quantified by a constant ratio (called the “leakiness” and denoted by ϵ) for the probability a previously infected individual will get infected upon exposure relative to a naively susceptible individual. We always assume that ϵ is between zero and one, with $\epsilon = 0$ corresponding to the SIR model and $\epsilon = 1$ corresponding to the SIS model.

A key concept in mathematical epidemiology is the basic reproduction number R_0 and its role as a threshold quantity. It is well-known that for a general family of compartmental disease models when $R_0 > 1$

we can expect a disease outbreak to occur [5,6]. For such models, this is a transcritical bifurcation point at which stability switches from the disease-free equilibrium to the endemic equilibrium. Gomes et al. [7] introduced a new threshold condition for a SIR model modified to have leaky immunity. They named this the reinfection threshold which occurs when the basic reproduction number is equal to $R_{0,\epsilon} = \frac{1}{\epsilon}$. They found that if vaccination generates the same level of leaky immunity as natural infection then the disease is controllable (by vaccinating the whole population) when $R_0 < R_{0,\epsilon}$. In this case $R_0 = R_{0,\epsilon}$ is associated with a transcritical bifurcation point. For the case with no vaccination, Gomes et al. [7] pointed out that the disease prevalence at the endemic equilibrium increases rapidly past the reinfection threshold. However, in this case, there is no bifurcation point, which led to a response letter by Breban and Blower [8] arguing against the proposed reinfection threshold. This response pointed out that the endemic equilibrium is globally stable if $R_0 > 1$ so that the only threshold phenomenon (which they define as the existence of a critical value at which there is a qualitative change in the dynamics of a system) that occurs is a transition from stable node to a stable spiral, and this transition point does not coincide with $R_{0,\epsilon}$. In response, Gomes et al. [9] clarified that while the bifurcation at the proposed threshold only occurs for the model with full vaccination, in the model without vaccination the

* Corresponding author.

E-mail address: felicia.magpantay@queensu.ca (F.M.G. Magpantay).

level of prevalence increases by orders of magnitude upon crossing the threshold, at least for their chosen parameter values.

The significance of the reinfection threshold in other models has also been further established. Stollenwerk et al. [10] considered a stochastic spatial disease model and showed that the reinfection threshold is associated with a critical threshold in the disease spread behavior (from annular to compact growth) in the limit when waning tends to zero. Martins et al. [11] extended the reinfection threshold to define the maximum curvature reinfection threshold which applies to systems with both leaky and waning immunity but no births or deaths. They showed that in the limit with no waning, this maximum curvature reinfection threshold coincides with the original reinfection threshold. Finally, Pagliara et al. [12] showed that the reinfection threshold is associated with a real dynamical regime change in the case with no waning and no births or deaths. We discuss the results of these papers further in Section 5.

The paper is organized as follows: In Section 2 we revisit the reinfection threshold from the original leaky model with no vaccination. In Section 3 we show that for all degrees of leakiness $\epsilon \in [0, 1]$, the endemic equilibrium starts off as a stable node after crossing $R_0 = 1$. In the case of the SIS model ($\epsilon = 1$) the equilibrium remains a stable node for all values of $R_0 > 1$. In the case of the SIR model ($\epsilon = 0$) the equilibrium becomes a stable spiral for an interval of R_0 values before returning to a stable node. For a leaky model with fixed $\epsilon \in (0, 1)$, we also show that the behavior is similar to the SIR model with a smaller interval over which the equilibrium is a spiral. We present a way to compute the point at which the endemic equilibrium changes back from a stable spiral to a stable node, and show that this can be approximated by the reinfection threshold when the recovery period from the disease is short relative to the lifetime of individuals in the population. On the other hand, in Section 4, we show that, again under the condition that the recovery period is short relative to lifetimes, the maximum rate of change in the prevalence of the disease relative to leakiness occurs close to the reinfection threshold. In Section 5 the connections between these analytic results and those of Stollenwerk et al. [10] and Martins et al. [11] are discussed. In Section 6 we considered a stochastic version of the leaky model (details available in uploaded code) and performed a simulation study to explore consequences of the reinfection threshold in practice. We show that using our default parameter values, the basic reproduction number values can be estimated more precisely when their values are lower than the value associated with the reinfection threshold.

2. The leaky model

Here we begin with a review of a simple SIR model with leaky infection-derived immunity. Some of the discussion and results are presented in the supplementary material. The numbering of sections and lemmas from the supplementary material are prefixed by an S.

We consider a modified compartmental SIR model with leaky infection-derived immunity given by the following system of equations,

$$\frac{dS}{dt} = \mu - \beta SI - \mu S, \tag{1}$$

$$\frac{dI}{dt} = \beta SI + \epsilon \beta RI - \gamma I - \mu I, \tag{2}$$

$$\frac{dR}{dt} = \gamma I - \epsilon \beta RI - \mu R. \tag{3}$$

Here S , I and R are the proportions of the population that are naively susceptible, infectious and recovered from the disease respectively. The parameter μ is the per capita birth and death rate, β is the transmission rate, γ is the recovery rate from the disease and ϵ is the leakiness parameter. If $\epsilon = 1$ we obtain the SIS model (nonexistent immunity) and if $\epsilon = 0$ we obtain the SIR model (perfect and lifelong immunity). The model parameters as well as their default values used for plots are given in Table 1. The model is illustrated in Fig. 1.

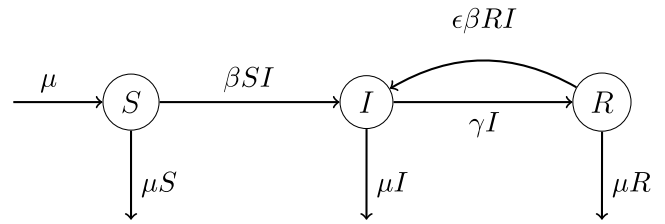


Fig. 1. The leaky model.

Table 1

Model parameters.

| Symbol | Description | Range | Default value |
|------------|----------------------|---------------|---------------------------------|
| μ | Birth and death rate | $(0, \infty)$ | $\frac{1}{70} \text{ yr}^{-1}$ |
| γ | Recovery rate | $(0, \infty)$ | $\frac{365}{8} \text{ yr}^{-1}$ |
| β | Transmission rate | $(0, \infty)$ | Varies |
| ϵ | Leakiness | $[0, 1]$ | 0.25 |

Table 2

Non-dimensional quantities obtained from model parameters.

| Symbol | Description | Formula | Range |
|--------|---------------------------|-------------------------------|---------------|
| R_0 | Basic reproduction number | $\frac{\beta}{\gamma + \mu}$ | $(0, \infty)$ |
| q | Probability of recovery | $\frac{\gamma}{\gamma + \mu}$ | $(0, 1)$ |

The set $S = \{(S, I, R) : S + I + R = 1, S \geq 0, I \geq 0, R \geq 0\}$ is invariant with respect to (1)–(3). When constrained to this set, the system of equations can be simplified using $R = 1 - S - I$ to,

$$\frac{dS}{dt} = \mu - \beta SI - \mu S, \tag{4}$$

$$\frac{dI}{dt} = \beta(S + \epsilon(1 - S - I))I - \gamma I - \mu I. \tag{5}$$

This can be transformed to the modified SIR system studied in [7] by scaling by the infectious period (see Section S1).

The basic reproduction number associated with the leaky model, computed using the next-generation matrix method [5,13], is $R_0 = \frac{\beta}{\gamma + \mu}$. This is the same as the reproduction number for the SIR and SIS models, and is unaffected by the leakiness parameter ϵ . Following [4], we also define the probability of recovery $q = \frac{\gamma}{\gamma + \mu}$. These non-dimensional parameters are listed in Table 2. It is convenient to use R_0 and q in place of β and γ for many of the longer expressions that we derive for this model. In this paper we assume that $\mu > 0$ is fixed and consider various dynamics of the model for $q \in (0, 1)$, $\epsilon \in [0, 1]$ and $R_0 > 0$, with a focus on $R_0 > 1$.

The system (4)–(5) has two equilibria: a disease-free equilibrium, $(S, I) = (1, 0)$, and an endemic equilibrium, $(S^*, I^*) = \left(\frac{\mu}{\mu + \lambda^*}, \frac{\lambda^*}{\beta}\right)$ where λ^* is the endemic equilibrium value of the force of infection $\lambda = \beta I$ and is given (in terms of μ , q , ϵ and R_0) by,

$$\lambda^* = \begin{cases} \mu(R_0 - 1), & \text{if } \epsilon = 0, \\ \mu \frac{\epsilon(R_0 + q - 1) - 1 + \sqrt{(\epsilon(R_0 + q - 1) - 1)^2 + 4(1 - q)\epsilon(R_0 - 1)}}{2(1 - q)\epsilon}, & \text{if } \epsilon \in (0, 1), \\ \frac{\mu(R_0 - 1)}{1 - q}, & \text{if } \epsilon = 1. \end{cases} \tag{6}$$

This expression for λ^* is continuous in ϵ on the closed interval $[0, 1]$. It coincides with the disease-free equilibrium at $R_0 = 1$ and is biologically feasible with $I^* > 0$ if $R_0 > 1$.

Next, we present the definition of the reinfection threshold which we revisit in this paper. This threshold was first introduced by Gomes et al. [7], and was the subject of back-and-forth discussion between Breban and Blower [8] and Gomes et al. [9]. Since we vary both R_0 and

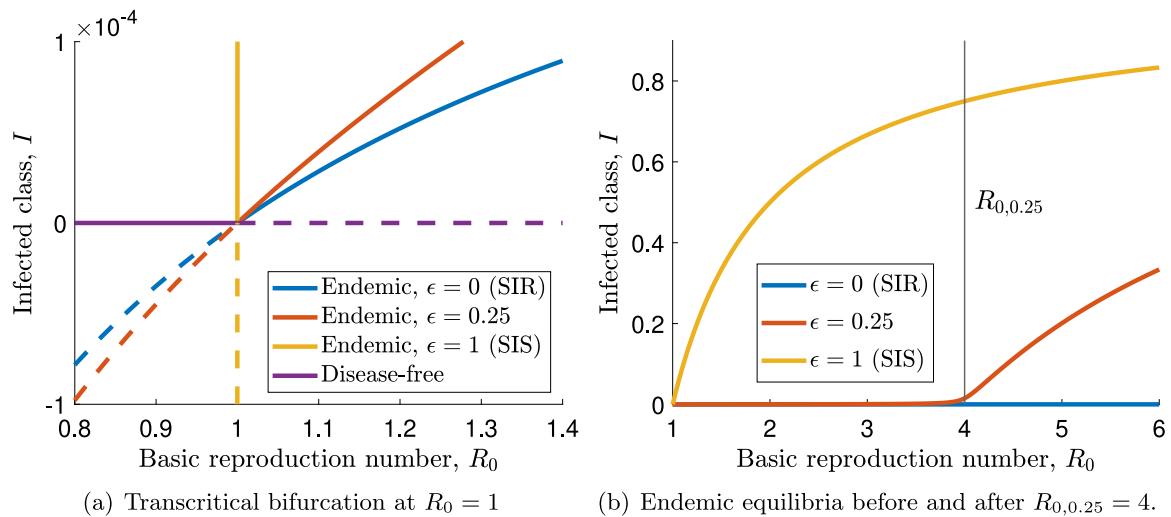


Fig. 2. The infected class component of equilibria versus the basic reproduction number R_0 . In (a), stable equilibria are denoted by solid lines and unstable are denoted by dashed lines.

ϵ in this paper, we specifically define both the reinfection threshold basic reproduction number value and the reinfection threshold leakiness value.

Definition 2.1 (Reinfection Threshold). As defined by Gomes et al. [7], the reinfection threshold of a leaky model occurs when $R_0 = \frac{1}{\epsilon}$. If the leakiness $\epsilon \in (0, 1]$ is fixed then the reinfection threshold basic reproduction number value is denoted by $R_{0,\epsilon} = \frac{1}{\epsilon}$. If the basic reproduction number value $R_0 > 1$ is fixed then the reinfection threshold leakiness value is $\frac{1}{R_0}$.

3. Spiral to node transition

It is easy to show that if $0 < R_0 < 1$ the disease-free equilibrium is globally asymptotically stable for initial conditions in S . If $R_0 > 1$ the disease-free equilibrium is unstable and the endemic equilibrium is globally asymptotically stable for initial conditions in S with $I > 0$ (refer to Section S2 in the supplementary file). Bifurcation diagrams for different values of leakiness are shown in Fig. 2. The transcritical bifurcation where the disease-free and endemic equilibria change stability is a feature of standard extensions of the SIR models. We are interested in qualitative changes in the dynamics of a leaky model past $R_0 = 1$. In Fig. 2(b) we see the behavior indicated by Gomes et al. [7] where the endemic equilibrium increases by orders of magnitude as R_0 is increased past its reinfection threshold value of $R_{0,\epsilon} = \frac{1}{\epsilon}$.

From (6), we see that the endemic equilibrium values of the force of infection and individual compartments vary with leakiness. However, as in [14], we can define an effective susceptible population given by $S_{\text{eff}} = S + \epsilon R = S + \epsilon(1 - S - I)$. This takes into account the fact that individuals in the R class are still partially susceptible to infection. We see that S_{eff}^* , the endemic equilibrium value of S_{eff} , is conserved for different values of ϵ . This is useful later on when we try to determine the dynamical behavior of solutions close to endemic equilibrium.

Theorem 3.1. For any $\epsilon \in [0, 1]$, at the endemic equilibrium (S^*, I^*) ,

$$S_{\text{eff}}^* = S^* + \epsilon(1 - S^* - I^*) = \frac{1}{R_0}.$$

Proof. Using $(S, I, R) = (S^*, I^*, R^*)$ in (2) in the original system, we derive $\beta S^* I^* + \epsilon \beta R^* I^* - \gamma I^* - \mu I^* = 0$. For $I^* \neq 0$, solving for $S^* + \epsilon R^*$ yields $S_{\text{eff}}^* = S^* + \epsilon R^* = \frac{\gamma + \mu}{\beta} = \frac{1}{R_0}$. \square

While the equilibrium value of S_{eff} is the same for all values of ϵ , the way this equilibrium value is approached varies depending on the eigenvalues of its Jacobian evaluated at the equilibrium [15,16]. For $R_0 > 1$, as we already discussed, the endemic equilibrium is stable so both eigenvalues must have negative real parts. If the eigenvalues form a complex conjugate pair with a negative real part among the eigenvalues then the equilibrium is a spiral and solutions approach the equilibrium via damped oscillations. Otherwise, both eigenvalues must be negative real numbers and the equilibrium is a stable node. In Fig. 3(a), we see that for $R_0 = 3$ the leaky model with $\epsilon = 0.25$ approaches equilibrium via decaying oscillations, similar to the corresponding SIR model. In Fig. 3(b) we see that for $R_0 = 5$ the leaky model with $\epsilon = 0.25$ approaches equilibrium without oscillations, similar to the corresponding SIS model. Figs. 3(a) and 3(b) compare the dynamics of the leaky model with $\epsilon = 0.25$ before and after its reinfection threshold of $R_{0,0.25} = 4$.

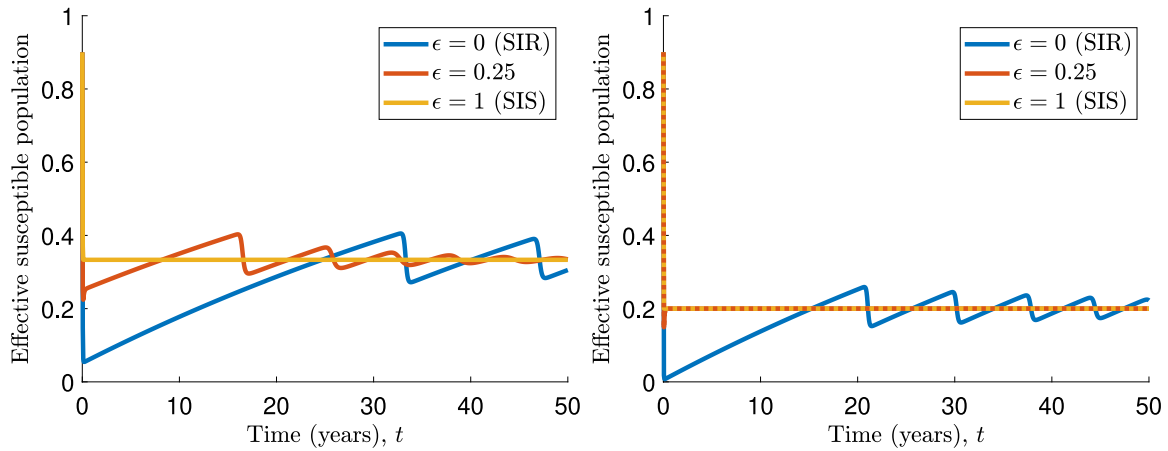
In Fig. 4, we compare the real and imaginary parts of the eigenvalues of the two-dimensional Jacobian matrix of (4)–(5) at the endemic equilibrium of the leaky model with $\epsilon = 0.25$ to the SIR and SIS models. The SIS model always has a pair of two negative real eigenvalues. For the range of R_0 values used in Fig. 4, the SIR model has a complex conjugate pair of eigenvalues. The form of the eigenvalues of the leaky model also depends on the value of R_0 . After crossing $R_0 = 1$ both of its eigenvalues are real and negative, but soon enough these eigenvalues form a complex conjugate pair. The imaginary parts disappear for later values of R_0 . We observe that the point at which the imaginary parts disappear is very close to the reinfection threshold of $R_{0,\epsilon} = \frac{1}{\epsilon}$ but, as noted by Breban and Blower [8], is not the same as the reinfection threshold.

The next results involve characterizing the dynamics of the models for all values of $R_0 > 1$. This involves Definition 3.2 and Theorem 3.3. In all of our results, we assume a fixed value of the birth/death rate $\mu > 0$ while we consider changing R_0, q and ϵ .

Definition 3.2. We define the following cubic polynomial in λ ,

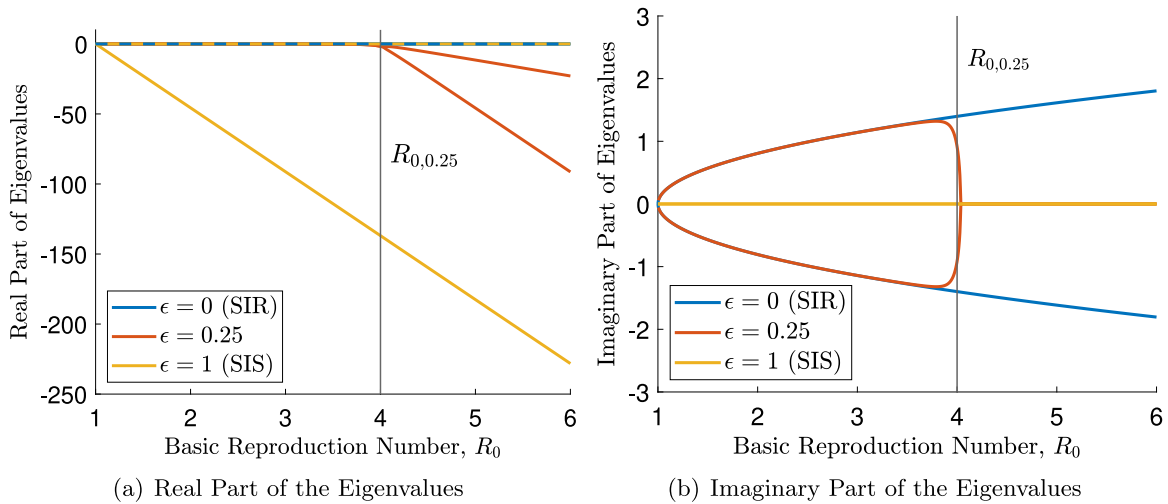
$$Z_{q,\epsilon}(\lambda) = (1 - q)((1 - \epsilon)\lambda + \mu)^2(\epsilon\lambda + \mu) - 4(1 - \epsilon)\mu\lambda((1 - q)\epsilon\lambda + \mu). \quad (7)$$

If $\epsilon \in (0, 1)$, by Lemma S5.2 this function has three distinct real roots $\lambda_0(q, \epsilon)$, $\lambda_1(q, \epsilon)$ and $\lambda_2(q, \epsilon)$ that continuously depend on $q \in (0, 1)$ and $\epsilon \in (0, 1)$ with the property that $\lambda_0(q, \epsilon) < 0 < \lambda_1(q, \epsilon) < \lambda_2(q, \epsilon)$. By Lemma S2.1, we can also define \mathcal{R}_1 and $\mathcal{R}_2 \in C((0, 1)^2, (1, \infty))$ given by



(a) Effective susceptible population for $R_0 = 3$. (b) Effective susceptible population for $R_0 = 5$.

Fig. 3. Effective susceptible population versus time using initial conditions $S(0) = 0.9$, $I(0) = 0.1$ and $R(0) = 0$. For $R_0 > 1$, the effective susceptible population has the same endemic equilibrium value of $\frac{1}{R_0}$ regardless of the value of ϵ . The transient dynamics depend on the values of R_0 and ϵ .



(a) Real Part of the Eigenvalues (b) Imaginary Part of the Eigenvalues

Fig. 4. The real part of the eigenvalues is always negative for $R_0 > 1$. The imaginary part is zero for the $\epsilon = 1$ (SIS) case. Whether the eigenvalues are purely real or form a complex conjugate pair depends on the parameter values (refer to Theorem 3.3).

$\mathcal{R}_j(q, \epsilon) = \mathcal{R}_{q,\epsilon}(\lambda_j(q, \epsilon))$ for $j = 1, 2$, where $\mathcal{R}_{q,\epsilon} \in C([0, \infty), [1, \infty))$ is the increasing function given by,

$$\mathcal{R}_{q,\epsilon}(\lambda) = \frac{(\lambda + \mu)((1 - q)\epsilon\lambda + \mu)}{\mu(\epsilon\lambda + \mu)}. \tag{8}$$

An exact formula for the three real roots of $Z_{q,\epsilon}(\lambda)$ is provided in Lemma S5.3. In practice, it is easier to use a numerical root-solver to find these roots than to apply the formula. The exact formula however becomes useful when we look for the limits as q approaches one, which we will see in a later theorem. The next theorem shows that $\mathcal{R}_j(q, \epsilon)$ for $j = 1, 2$ provide the endpoints of the interval over which a leaky model with $\epsilon \in (0, 1)$ is a stable spiral.

Theorem 3.3. *The following statements hold:*

1. The endemic equilibrium of the SIS model ($\epsilon = 1$) is a stable node for all $R_0 > 1$;
2. The endemic equilibrium of the SIR model ($\epsilon = 0$) is a stable spiral for $R_0 \in \left(\frac{2}{1+\sqrt{q}}, \frac{2}{1-\sqrt{q}}\right) \subset (1, \infty)$. It is a stable node for all other values of $R_0 > 1$;
3. The endemic equilibrium of the leaky model with $\epsilon \in (0, 1)$ is a stable spiral for $R_0 \in (\mathcal{R}_1(q, \epsilon), \mathcal{R}_2(q, \epsilon)) \subset (1, \infty)$ where \mathcal{R}_1 and \mathcal{R}_2 are

the functions given in Definition 3.2. It is a stable node for all other values of $R_0 > 1$.

To prove Theorem 3.3 we first find the Jacobian matrix associated with (4)–(5) evaluated at the endemic equilibrium (S^*, I^*) ,

$$J(S^*, I^*) = \begin{bmatrix} -\lambda^* - \mu & -\frac{\mu^2 R_0}{(1-q)(\lambda^* + \mu)} \\ (1-\epsilon)\lambda^* & -\epsilon\lambda^* \end{bmatrix}. \tag{9}$$

This can be derived using Theorem 3.1. Refer to Section S3 in the supplementary file for details. We already know that the eigenvalues of the Jacobian all have negative real parts for $R_0 > 1$ [5,6]. Here we are just looking for when the eigenvalues form a complex conjugate pair.

Proof of 1. Setting $\epsilon = 1$ and $\lambda^* = \frac{\mu(R_0-1)}{1-q}$ simplifies the Jacobian so that it is easy to see that the eigenvalues are $-\frac{\mu(R_0-q)}{1-q}$ and $-\frac{\mu(R_0-1)}{1-q}$. This shows that for all $R_0 > 1$ the endemic equilibrium is a stable node. \square

Proof of 2. Setting $\epsilon = 0$ and $\lambda^* = \mu(R_0 - 1)$ in (9) and solving for the discriminant $\Delta = \text{Tr}(J)^2 - 4\text{Det}(J)$ yields,

$$\Delta = \mu^2 \left(R_0^2 - \frac{4(R_0 - 1)}{1 - q} \right). \tag{10}$$

The graph of Δ as a function of R_0 is a concave up parabola with roots at $R_0 = \frac{2}{1 \pm \sqrt{q}}$. Thus, the endemic equilibrium of the SIR model is stable node everywhere except for the interval over which this parabola is negative which is given by $(\frac{2}{1+\sqrt{q}}, \frac{2}{1-\sqrt{q}})$. On this interval, it is a stable spiral. \square

Proof of 3. In this case, it is convenient to find the discriminant Δ in terms of λ^* instead of R_0 . From Lemma S2.1 we can set $R_0 = \mathcal{R}_{q,\epsilon}(\lambda^*)$ in (9). Solving for the discriminant $\Delta = \text{Tr}(J)^2 - 4\text{Det}(J)$ and simplifying, yields $\Delta = ((1-\epsilon)\lambda^* + \mu)^2 - \frac{4(1-\epsilon)\mu\lambda^*((1-q)\epsilon\lambda^* + \mu)}{(1-q)(\epsilon\lambda^* + \mu)}$. This has the same sign as $Z_{q,\epsilon}(\lambda^*)$ for all $\lambda^* > 0$ (refer to Section S4 for details). In particular, $Z_{q,\epsilon}(\lambda^*)$ and Δ have the same signs for all $\lambda^* \geq 0$.

From Definition 3.2, we know that there are three distinct roots of $Z_{q,\epsilon}(\lambda)$, given by $\lambda = \lambda_i(q, \epsilon)$, $i = 0, 1, 2$, where $\lambda_0(q, \epsilon) < 0 < \lambda_1(q, \epsilon) < \lambda_2(q, \epsilon)$. Since $Z_{q,\epsilon}(\lambda)$ has a positive leading order term, for non-negative values of λ , $Z_{q,\epsilon}(\lambda)$ is only negative in the interval $(\lambda_1(q, \epsilon), \lambda_2(q, \epsilon))$. This interval maps to $(\mathcal{R}_1(q, \epsilon), \mathcal{R}_2(q, \epsilon))$ using the function $\mathcal{R}_{q,\epsilon}(\lambda)$. \square

Remark 3.4. For the SIR model, we can see that when q is close to one, the left endpoint is very close to $R_0 = 1$ while the right endpoint is very large. In this case, for most reasonable $R_0 > 1$ values the endemic equilibrium of the SIR model is a stable spiral and that of the SIS model is a stable node. Thus, for q close to one, when the value of R_0 crosses the reinfection threshold we can think of the behavior of the dynamics transitioning suddenly from SIR-like to SIS-like behavior.

Definition 3.2 and Theorem 3.3 allow us to compute the exact interval over which the complex conjugate pair of eigenvalues to the Jacobian exist for a leaky model with $\epsilon \in (0, 1)$. The next two theorems provide some intuition on the interval and how it relates to the reinfection threshold. In Theorem 3.5 we provide some bounds on the endpoints of the interval. In Theorem 3.6 we show that the left endpoint approaches one and the right endpoint approaches the reinfection threshold reproduction number value when the recovery rate from the disease is assumed to be much faster than the expected individual lifetime.

Theorem 3.5. Let $q \in (0, 1)$ and $\epsilon \in (0, 1)$. Then $\mathcal{R}_1(q, \epsilon)$, the left endpoint of the R_0 -interval over which the leaky model is a spiral, has the following bounds,

$$\mathcal{R}_{q,\epsilon} \left(\frac{\mu(1-q)}{4(1-\epsilon)} \right) < \mathcal{R}_1(q, \epsilon) < \mathcal{R}_{q,\epsilon} \left(\frac{\mu(1-q)(6-5\epsilon-q(2-\epsilon))}{16(1-\epsilon)^2} \right). \quad (11)$$

Proof. This follows from Lemma S5.2 and Lemma S2.1. \square

The next theorem shows that in the limit when $q \rightarrow 1^-$, $\mathcal{R}_1(q, \epsilon)$ approaches one and $\mathcal{R}_2(q, \epsilon)$ approaches the $R_{0,\epsilon} = \frac{1}{\epsilon}$, the reinfection threshold value of the basic reproduction number (see also Fig. 5).

Theorem 3.6. Let $\epsilon \in (0, 1)$. The following statements hold:

1. $\lim_{q \rightarrow 1^-} \mathcal{R}_1(q, \epsilon) = 1$;
2. $\lim_{q \rightarrow 1^-} \mathcal{R}_2(q, \epsilon) = \frac{1}{\epsilon}$.

Proof of Part 1. This follows from Theorem 3.5 part 1, the continuity of $\mathcal{R}_{q,\epsilon}(\lambda)$ and the squeeze theorem on the limit as $q \rightarrow 1^-$. \square

Proof of Part 2. From Lemma S5.3 we have that for q close enough to 1 (from below),

$$\lambda_2(q, \epsilon) = \ell_0(q, \epsilon) = \frac{1}{3\epsilon(1-\epsilon)} \left[2 \left(\frac{\rho}{1-q} \right)^{1/3} \cos \left(\frac{\theta}{3} \right) + 3\epsilon - 1 \right] \mu, \quad (12)$$

where $\rho(q, \epsilon) = |\zeta(q, \epsilon)|$, $\theta(q, \epsilon) = \text{atan2}(\text{Im}(\zeta(q, \epsilon)), \text{Re}(\zeta(q, \epsilon)))$,

$$\zeta(q, \epsilon) = 18q\epsilon(1-\epsilon)(3\epsilon-1) + q-1 - 6\epsilon\sqrt{q(q,\epsilon)i}, \quad \text{where } i = \sqrt{-1},$$

$$\alpha(q, \epsilon) = 3q(1-\epsilon) \left[\frac{16\epsilon(1-\epsilon)^2}{1-q} + (1-\epsilon)(5\epsilon^2 - 14\epsilon + 1) - (1-q)\epsilon(11\epsilon^2 - 13\epsilon + 1) \right].$$

We note that $\alpha \in O((1-q)^{-1})$ which means $\zeta \in O((1-q)^{-1/2})$, $\rho \in O((1-q)^{-1/2})$ and $\lambda_2 \in O((1-q)^{-1/2})$. From (8),

$$\begin{aligned} \lim_{q \rightarrow 1^-} \mathcal{R}_2(q, \epsilon) &= \lim_{q \rightarrow 1^-} \mathcal{R}_{q,\epsilon}(\lambda_2(q, \epsilon)) \\ &= \lim_{q \rightarrow 1^-} \frac{(\lambda_2(q, \epsilon) + \mu)((1-q)\epsilon\lambda_2(q, \epsilon) + \mu)}{\mu(\epsilon\lambda_2(q, \epsilon) + \mu)}, \\ &= \lim_{q \rightarrow 1^-} \frac{(1 + \frac{\mu}{\lambda_2(q,\epsilon)})((1-q)\epsilon\lambda_2(q, \epsilon) + \mu)}{\mu(\epsilon + \frac{\mu}{\lambda_2(q,\epsilon)})}. \end{aligned} \quad (13)$$

Since $\lambda_2 \in O((1-q)^{-1/2})$, we have that $\lim_{q \rightarrow 1^-} \frac{\mu}{\lambda_2(q,\epsilon)} = 0$ and $\lim_{q \rightarrow 1^-} (1-q)\epsilon\lambda_2(q, \epsilon) = 0$. Using this in (13) yields $\lim_{q \rightarrow 1^-} \mathcal{R}_2(q, \epsilon) = \frac{(1+0)(0+\mu)}{\mu(\epsilon+0)} = \frac{1}{\epsilon}$ as required. \square

4. Maximum rate of change of prevalence with respect to leakiness

Gomes et al. [9] highlighted that the endemic equilibrium value of the infectious compartment increases rapidly upon crossing the reinfection threshold. In Fig. 6, we show that the rapid change in the endemic equilibrium value of the force of infection (which is proportional to prevalence) does occur when q is close to one, however, the change is less dramatic when q is not as close to one. The point at which the force of infection is changing most rapidly with respect to ϵ is the inflection point in the graph of Fig. 6(a).

Definition 4.1. By Lemma S6.1, for any $R_0 > 1$ and $q \in (0, 1)$ we can define the following $C^1([\mu(R_0-1), \frac{\mu(R_0-1)}{1-q}], [0, 1])$ function given by,

$$\mathcal{E}_{q,R_0}(\lambda) = \frac{\mu(\lambda + \mu) - \mu^2 R_0}{\mu\lambda R_0 - (1-q)\lambda(\lambda + \mu)} \quad (14)$$

Lemma S6.1 also states that we can define the following $C((0, 1) \times (1, \infty), [\mu(R_0-1), \frac{\mu(R_0-1)}{1-q}])$ function,

$$\tilde{\lambda}(q, \epsilon) = \underset{\lambda \in [\mu(R_0-1), \frac{\mu(R_0-1)}{1-q}]}{\text{argmin}} \frac{d\mathcal{E}_{q,R_0}(\lambda)}{d\lambda}, \quad (15)$$

and the following $C((0, 1) \times (1, \infty), [0, 1])$ function,

$$\tilde{\mathcal{E}}(q, R_0) = \mathcal{E}_{q,R_0}(\tilde{\lambda}(q, R_0)). \quad (16)$$

By the definition of $\tilde{\lambda}(q, \epsilon)$, $\tilde{\mathcal{E}}(q, R_0)$ and the inverse function theorem, $\tilde{\mathcal{E}}(q, R_0)$ is the value of leakiness that corresponds to the largest rate of increase of the endemic equilibrium force of infection λ^* . This is illustrated in Fig. 6(a). A plot of $\tilde{\mathcal{E}}(q, R_0)$ as a function of the probability of recovery q is shown in Fig. 6(b). In the next theorem we prove that as $q \rightarrow 1^-$, $\tilde{\mathcal{E}}(q, R_0)$ approaches the reinfection threshold leakiness value of $\frac{1}{R_0}$.

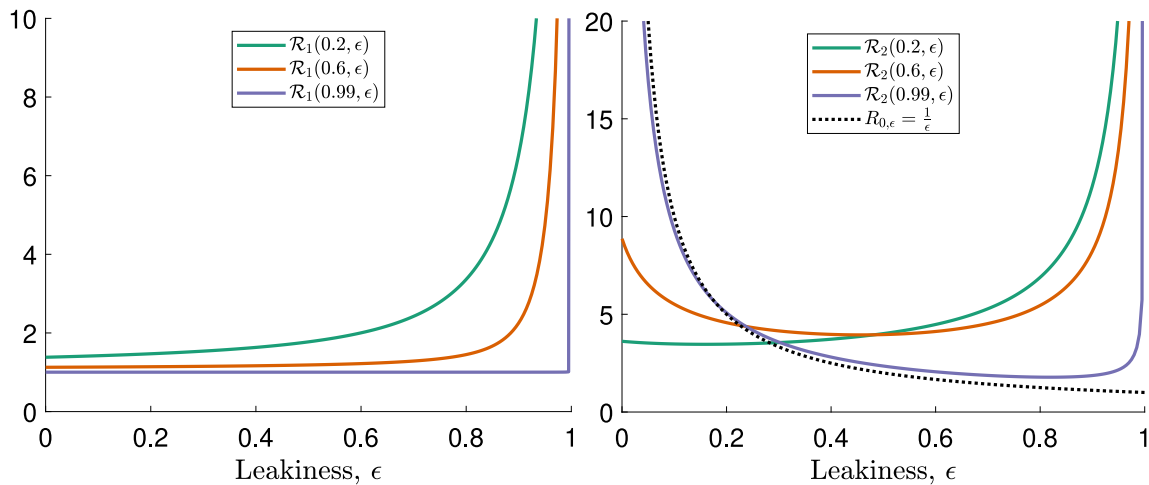
Theorem 4.2. For $q \in (0, 1)$ and $R_0 > 1$,

$$\tilde{\lambda}(q, \epsilon) = \begin{cases} \mu(R_0 - 1), & \text{if } q \in \left[0, \frac{R_0-1}{2R_0-1} \right], \\ (x^2 - xy + y^2)y\mu, & \text{if } q \in \left(\frac{R_0-1}{2R_0-1}, 1 \right], \end{cases} \quad (17)$$

and

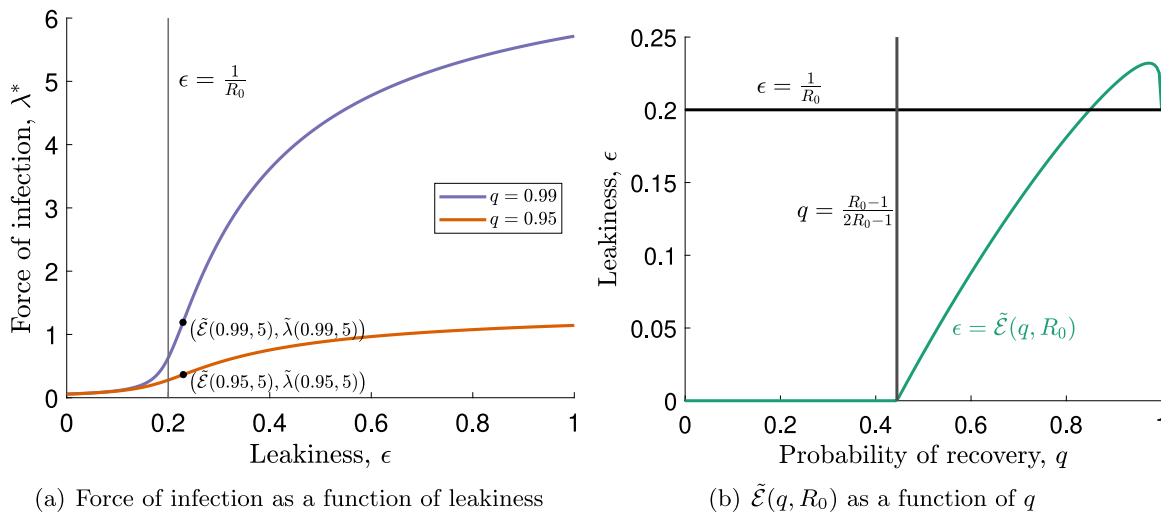
$$\tilde{\mathcal{E}}(q, \epsilon) = \begin{cases} 0, & \text{if } q \in \left[0, \frac{R_0-1}{2R_0-1} \right], \\ \mathcal{E}_{q,R_0}((x^2 - xy + y^2)y\mu), & \text{if } q \in \left(\frac{R_0-1}{2R_0-1}, 1 \right], \end{cases} \quad (18)$$

where $x = \left(\frac{R_0 q}{1-q} \right)^{1/3}$ and $y = (R_0 - 1)^{1/3}$.



(a) $\mathcal{R}_1(q, \epsilon)$, the lower bound of the R_0 interval for which the endemic equilibrium is a stable spiral. (b) $\mathcal{R}_2(q, \epsilon)$, the upper bound of the R_0 interval for which the endemic equilibrium is a stable spiral.

Fig. 5. Plots of $\mathcal{R}_1(q, \epsilon)$ and $\mathcal{R}_2(q, \epsilon)$ over $\epsilon \in (0, 1)$ for different values of q . We note that $\lim_{\epsilon \rightarrow 0^+} \mathcal{R}_1(q, \epsilon) = \frac{2}{1+\sqrt{q}}$, $\lim_{\epsilon \rightarrow 1^-} \mathcal{R}_1(q, \epsilon) = \infty$, $\lim_{\epsilon \rightarrow 0^+} \mathcal{R}_2(q, \epsilon) = \frac{2}{1-\sqrt{q}}$, $\lim_{\epsilon \rightarrow 1^-} \mathcal{R}_2(q, \epsilon) = \infty$, consistent with the properties of the SIR and SIS models given in Theorem 3.3. The reinfection threshold $R_{0,\epsilon}$ from [7] is also plotted in (b).



(a) Force of infection as a function of leakiness

(b) $\tilde{\mathcal{E}}(q, R_0)$ as a function of q

Fig. 6. (a) The force of infection of the leaky model at the endemic equilibrium for fixed $R_0 = 5$ and varying ϵ . From (6), at $\epsilon = 0$ all values are equal to $\mu(R_0 - 1)$ while at $\epsilon = 1$ the values are equal to $\frac{\mu(R_0 - 1)}{1 - q}$. (b) A plot of $\tilde{\mathcal{E}}(q, R_0)$ versus the probability of reinfection q . This approaches $\frac{1}{R_0}$ as $q \rightarrow 1^-$.

Proof. This follows from the results of Lemma S6.2 and the definition of $\mathcal{E}_{q,R_0}(\lambda)$ in Definition 4.1. \square

Theorem 4.3. For $R_0 > 1$,

$$\lim_{q \rightarrow 1^-} \tilde{\mathcal{E}}(q, R_0) = \frac{1}{R_0}. \tag{19}$$

Proof. By Theorem 4.2, for q close to 1 we have $\tilde{\lambda}(q, \epsilon) = (x^2 - xy + y^2)y\mu$, where $x = \left(\frac{R_0 q}{1 - q}\right)^{1/3}$ and $y = (R_0 - 1)^{1/3}$. Since $x \in O((1 - q)^{-1/3})$ then $\tilde{\lambda}(q, \epsilon) \in O((1 - q)^{-2/3})$ and $(1 - q)(\tilde{\lambda}(q, \epsilon) + \mu) \in O((1 - q)^{1/3})$. Thus,

$$\begin{aligned} \lim_{q \rightarrow 1^-} \tilde{\mathcal{E}}(q, R_0) &= \lim_{q \rightarrow 1^-} \mathcal{E}_{q,R_0}(\tilde{\lambda}(q, \epsilon)) \\ &= \lim_{q \rightarrow 1^-} \frac{\mu(\tilde{\lambda}(q, \epsilon) + \mu) - \mu^2 R_0}{\mu \tilde{\lambda}(q, \epsilon) R_0 - (1 - q)\tilde{\lambda}(q, \epsilon)(\tilde{\lambda}(q, \epsilon) + \mu)} \\ &= \lim_{q \rightarrow 1^-} \frac{\mu(1 + \frac{\mu}{\tilde{\lambda}(q, \epsilon)}) - \frac{\mu^2 R_0}{\tilde{\lambda}(q, \epsilon)}}{\mu R_0 - (1 - q)\tilde{\lambda}(q, \epsilon) + \mu} \\ &= \lim_{q \rightarrow 1^-} \frac{\mu(1 + 0) - 0}{\mu R_0 - 0} \end{aligned}$$

$$= \frac{1}{R_0}. \quad \square$$

The last theorem shows that the rapid change in the endemic equilibrium value of the force of infection occurs near the reinfection threshold when q is close to 1. Since $q = \frac{\gamma}{\gamma + \mu}$, the condition that q is close to one is easily satisfied when modeling acute infections where the recovery period from the disease is much shorter than the average lifetime.

5. Reinfection threshold in other models

In this section, we discuss how our results are connected to other results on the reinfection threshold, which were applied to different transmission models with leaky infection-derived immunity. Stollenwerk et al. [10] demonstrated that a phase transition in the growth of the epidemic is associated with the reinfection threshold value in a spatial, stochastic model of disease spread with no births and deaths. To gain some insight into the effect of this threshold in a mean field model, they incorporated the waning of immunity by allowing recovered individuals to move to the susceptible class. In this section we compare our

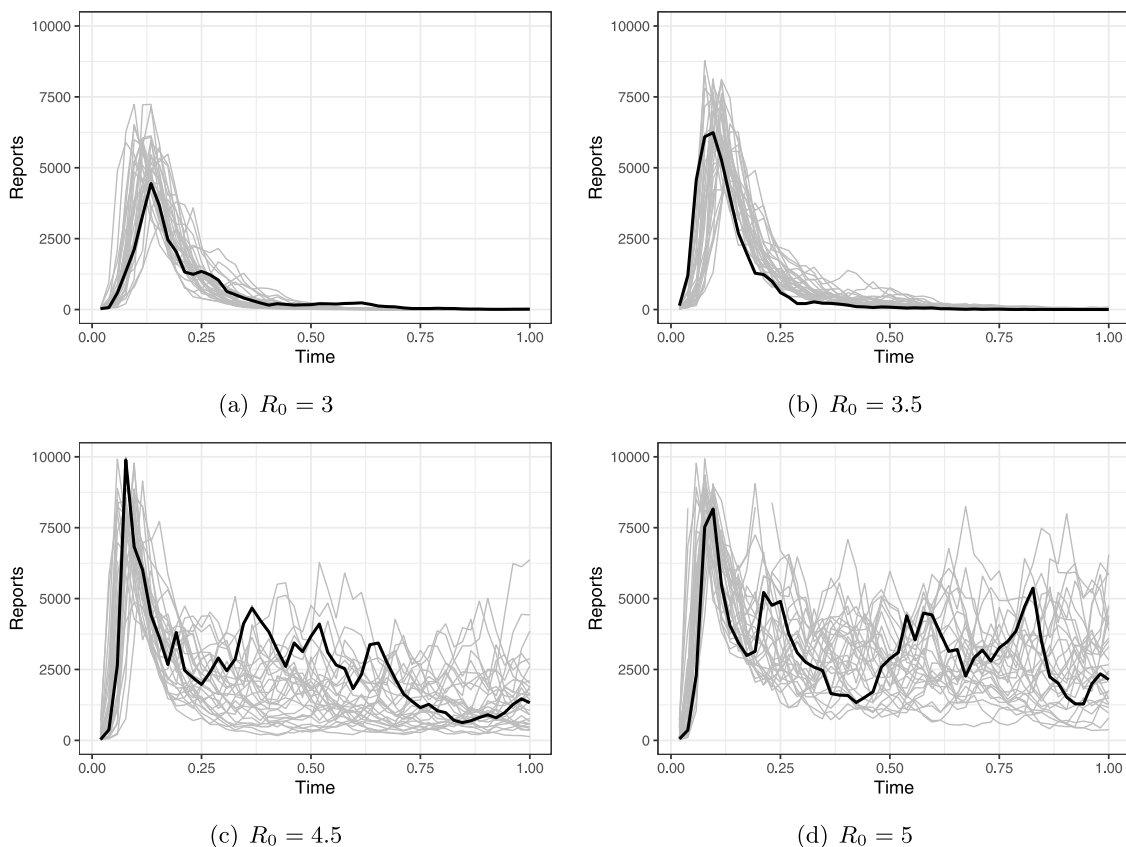


Fig. 7. Thirty sample simulations (out of a total of 300 sample simulations used) for each true value of R_0 . The values of ϵ , μ and γ used in the simulation are given in Table 1. Reporting probability was assumed to be 20%. The transmission rate was assumed to have multiplicative gamma white noise with intensity 0.05. The total population was assumed to be 100,000 with 0.1% infected at the initial time and everyone else susceptible.

results in that specific mean field model used by Stollenwerk et al. [10], which was also used by Martins et al. [11], to generalize the reinfection threshold concept. For clarity of exposition, we begin by setting up a general model with both leaky and waning immunity given by,

$$\frac{dS}{dt} = \mu + \alpha R - \beta SI - \mu S, \tag{20}$$

$$\frac{dI}{dt} = \beta SI + \epsilon \beta RI - \gamma I - \mu I, \tag{21}$$

$$\frac{dR}{dt} = \gamma I - \epsilon \beta RI - \alpha R - \mu R. \tag{22}$$

Our original leaky model (1)–(3) can be derived from this model by setting $\alpha = 0$. The mean-field model with reintroduced susceptibles discussed in [10,11] that we consider is (20)–(22) with $\alpha > 0$ and $\mu = 0$. Stollenwerk et al. [10] found that a sharp transition in the endemic equilibrium value of the infected class as a function of R_0 occurs as $\alpha \rightarrow 0^+$. Martins et al. [11] considered the same model and derived a more general quantity, the maximum curvature reinfection threshold, which is the R_0 value for which the endemic equilibrium value of the infected class attains its maximum curvature. Martins et al. [11] showed that this coincides with the reinfection threshold when $\alpha \rightarrow 0^+$. In particular, at this limit, there is a sharp transition as the curvature diverges to infinity.

The results on maximum curvature have similarities with the results we proved in Section 4. These results both imply that for q close to one the disease prevalence increases rapidly when R_0 goes beyond the reinfection threshold. However, in our case, we set $\mu > 0$, $\alpha = 0$ and consider the maximum rate of change of the endemic equilibrium value of the infected class relative to leakiness ϵ instead of R_0 , and we found that this point coincides with the reinfection threshold value of ϵ as $q = \frac{\gamma}{\gamma + \mu} \rightarrow 1^-$. We note that q is close to one when γ becomes large relative to μ , which can be interpreted as an acute infection where the

Table 3 Estimation of R_0 in the simulation study. For each true value of R_0 we generated 300 simulations, and for each simulation, we derived a maximum likelihood estimate (MLE) of R_0 and a 95% confidence interval (CI) using profile likelihood. The table shows the mean and standard deviation of the MLE distributions as well as the coverage of true value and CI mean length. Note that to limit computational cost, the confidence intervals are limited to be between $R_0 = 1.5$ to 8.

| True R_0 | R_0 MLE mean | R_0 MLE S.D. | Coverage | CI length mean |
|------------|----------------|----------------|----------|----------------|
| 3.00 | 3.10 | 0.51 | 0.95 | 2.04 |
| 3.50 | 3.61 | 0.66 | 0.95 | 2.66 |
| 4.50 | 4.68 | 0.95 | 0.95 | 3.61 |
| 5.00 | 5.21 | 1.14 | 0.93 | 3.76 |

recovery period is much shorter than the average lifetime of individuals in the population. However, to connect our results with [10,11], we can also instead think of $q \rightarrow 1^-$ occurring when we let $\mu \rightarrow 0^+$. Thus the results we proved in this paper can be thought of as applying to the case $\alpha = 0$ and $\mu \rightarrow 0^+$. On the other hand, the results we discussed above from [10,11] yield the reinfection threshold when setting $\mu = 0$ and $\alpha \rightarrow 0^+$.

The special case with $\alpha = 0$ and $\mu = 0$ connects [10,11] and our work. The properties of this specific case of (20)–(22) have been established in Pagliara et al. [12]. While in our work we restricted $\epsilon \in [0, 1]$, Pagliara et al. [12] considered a model wherein $\epsilon \in (0, \infty)$, which allows for “compromised immunity” (wherein recovered individuals are more likely to get infected than naively susceptible individuals). Since there is no reintroduction of susceptibles via either birth or waning immunity, the susceptible population decays to zero as $t \rightarrow \infty$ for any initialization with a nonzero infectious population. Instead of two distinct isolated equilibria, this case has a continuum of disease-free equilibria, $\{(S, I) = (S, 0) : S \in [0, 1]\}$, and one

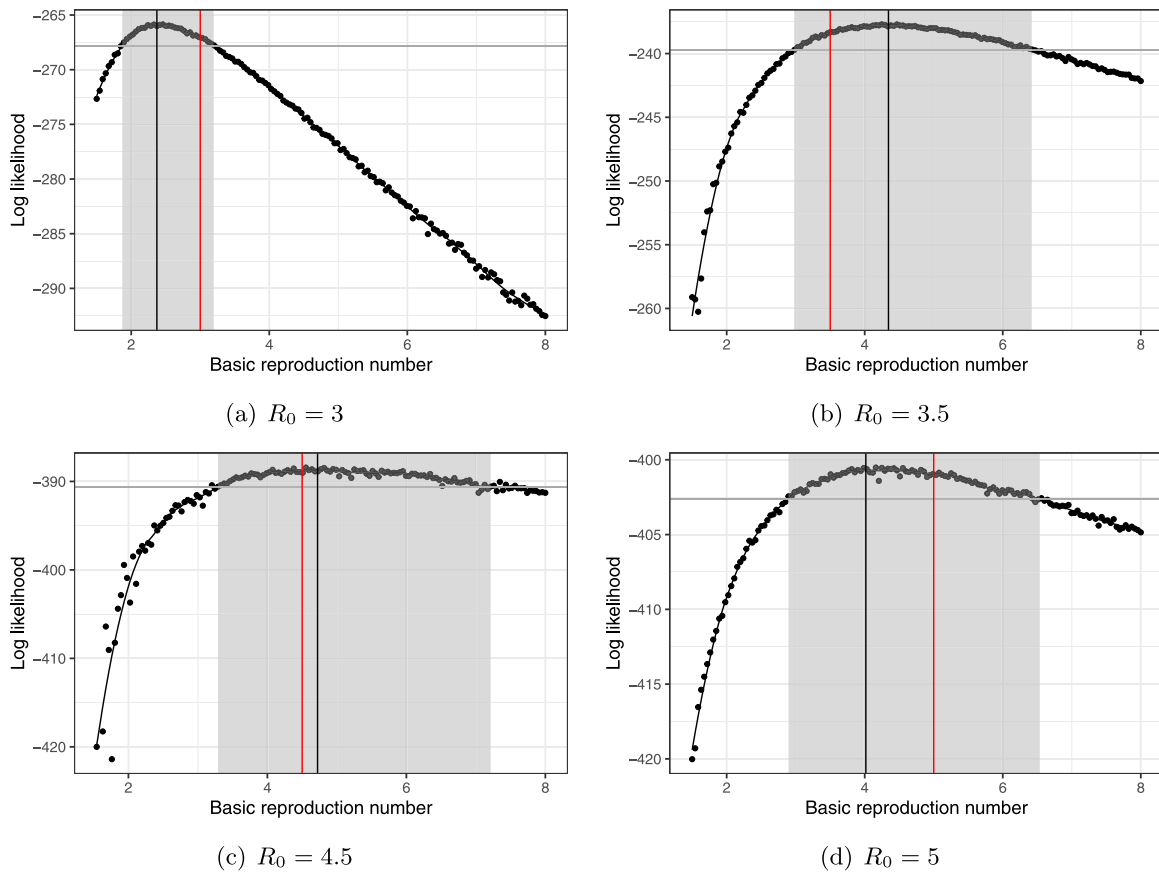


Fig. 8. Profiles over the basic reproduction number for the corresponding highlighted sample simulations Fig. 7. The black vertical lines indicate the ML estimate and the shaded areas show the 95% confidence intervals computed using profile likelihood. The true value of R_0 used in each simulation is indicated by the red vertical line.

endemic equilibrium, $(S, I) = (0, 1 - \frac{1}{\epsilon R_0})$. Pagliara et al. [12] found four dynamically different parameter regimes for trajectories initialized with $S(0) \in [0, 1)$ and $I(0) \in (0, 1]$:

1. If $R_0 < 1$ and $\epsilon R_0 < 1$ then trajectories approach a disease-free equilibrium via a monotonic decay in infections.
2. If $R_0 > 1$ and $\epsilon R_0 > 1$ then trajectories approach the endemic equilibrium.
3. If $R_0 > 1$ and $\epsilon R_0 \leq 1$ then trajectories approach a disease-free equilibrium. Depending on initial conditions, this occurs via monotonic decay in infections or after a single epidemic.
4. If $R_0 \leq 1$ and $\epsilon R_0 > 1$ then trajectories either approach a disease-free equilibrium or the endemic equilibrium depending on initializations.

Case 4, the case with bistable disease-free and endemic asymptotic dynamics is not possible under our assumption in this paper that $\epsilon \in [0, 1]$. However, it is important to note that the boundary case $\epsilon R_0 = 1$ separating some of these dynamically different regimes corresponds to the reinfection threshold. The sharp transitions we observe near the reinfection threshold at the limits considered in [10,11] and this paper, including the spiral to node transition, are related to the regime transitions in the special case of the model discussed in [12].

6. Parameter identifiability

In this section, we consider whether the reinfection threshold has an effect on parameter identifiability. To do this, we converted the leaky model to a discrete-state, continuous-time Markov chain with the same mean transition rates as those given in (1)–(3). We also used incorporated a multiplicative gamma white noise term (with mean

one and intensity 0.05) to the transmission rate, assumed Poisson distributed births into the susceptible class, and set all other transitions to be implemented using Euler multinomial draws over time intervals of length equal to 0.1 days. The model was implemented using the Partially Observed Markov Process (pomp) R package [17,18]. The S , I and R compartments of the model, as well as the true number of weekly recoveries from the disease (computed as the number of transitions from I to R) comprised the unobserved states of the model. The only observed state was the number of weekly reported cases of the disease. For the reporting model, we assume that the true number of cases that can be reported each week is approximated by the number of recoveries that week, similar to the reporting models used for acute infections in other studies [19]. This comes from the assumption that individuals need to experience some symptoms first before they get tested for a disease and that testing takes time, with the time from the start of the infection to the recording of the case being similar to the infectious period (which we fixed to be 8 days as in Table 1). We also assume each case independently has a 20% probability of being recorded, resulting in a binomial reporting model with a 20% reporting probability. All code and simulated datasets used for this simulation study is available online at <https://doi.org/10.5061/dryad.cc2fqz6c3>.

We fixed the values of μ , γ and ϵ to their default values in Table 1 with corresponding reinfection threshold basic reproduction number value of $R_{0,0.25} = 4$. We considered four β values corresponding to four R_0 values, two of which are smaller than $R_{0,0.25}$ and two that are larger (refer to Table 3). For each true value of R_0 , we generated 300 simulated time series of reported cases over one year (52 weekly reports) and profiled over R_0 for each simulation.

The profiles over R_0 we generated using the following procedure: The values of μ and γ were fixed to their true values. We set up

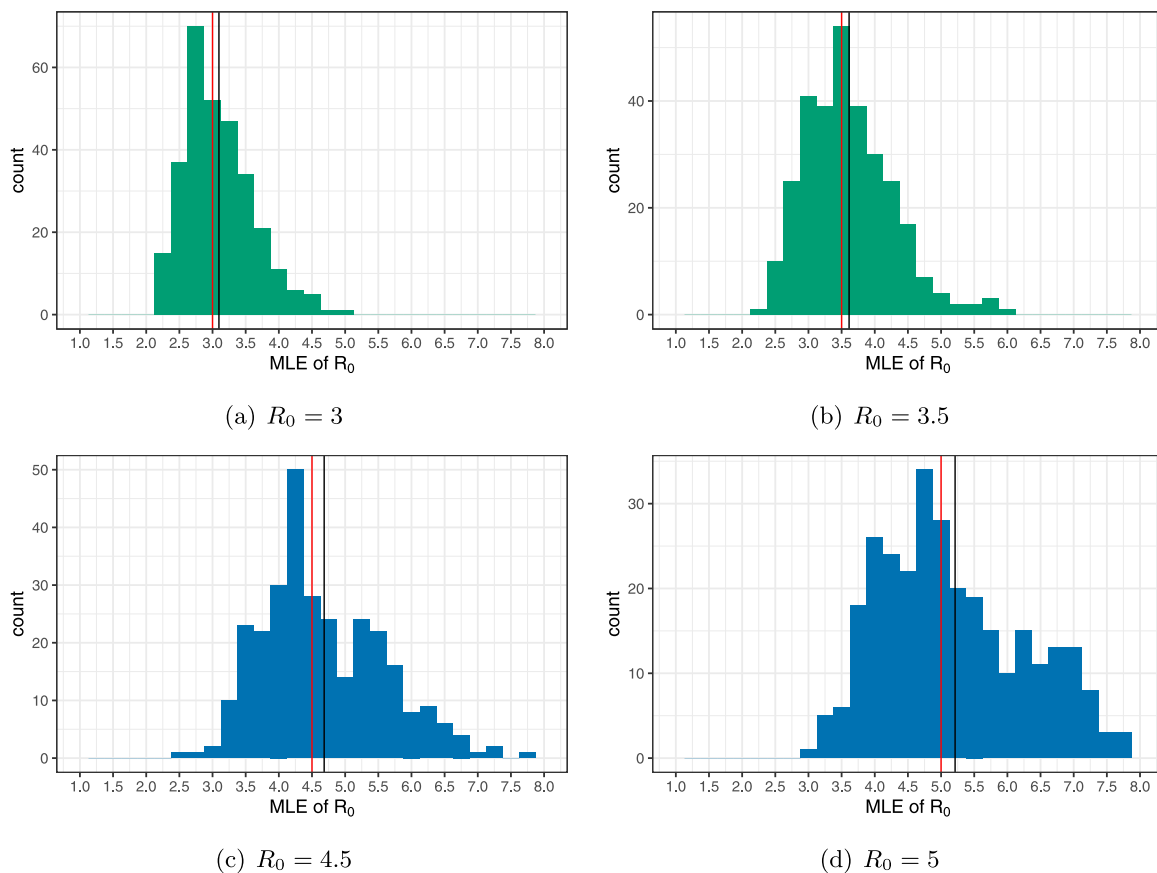


Fig. 9. Distribution of the MLEs for R_0 using profile likelihood for simulations generated with reproduction number values $R_0 < \frac{1}{\epsilon}$ for (a)–(b) and $R_0 > \frac{1}{\epsilon}$ for (c)–(d). The true value of R_0 is marked by the vertical red lines and the mean value of each distribution of ML estimates is denoted by vertical black lines.

an array of 150 values of R_0 equally spaced from $R_0 = 1.5$ to 8. For each simulation and for each value of R_0 we searched for the maximum likelihood (ML) estimate of ϵ using the maximization via iterated filtering algorithm (`mif2`) in `pomp` [17] with 6000 particles, 50 iterations, initial random walk of 0.1 for the ϵ parameter (in the logit scale) and a final cooling fraction of 0.1. The likelihood associated with the algorithm’s ML estimate for ϵ for each fixed R_0 was then computed using the particle filter (`pfilter`) in `pomp` [17] with 12,000 particles and 10 repetitions. For each simulation, we generated a smoothed curve for profiles of likelihood versus R_0 using `loess` in R with $\alpha = 0.2$. The ML estimate for R_0 and its 95% confidence intervals were then computed using profile likelihood and loess curve fitting. As a result, for each simulation, we had a maximum likelihood estimate for R_0 and a 95% confidence interval (limited to be between $R_0 = 1.5$ and 8). A few sample simulations are plotted in Fig. 7 and sample profiles over R_0 corresponding to each highlighted simulation are shown in Fig. 8. The sample plots of the profiles suggest good convergence of both the maximization via iterated filtering and the particle filter for the settings used for both algorithms, and a good fit of the loess curve. The plots also show the maximum likelihood estimate (MLE) for R_0 (indicated by vertical black lines), the true value (indicated by vertical red lines) and the 95% confidence intervals shaded in gray. In both sample plots shown, the true value lies inside the confidence interval. This was true for the majority of the simulations, but not all. We computed the coverage, the proportion of simulations for which the true value of R_0 lies in the 95% confidence intervals, and the results for both the before and after threshold cases were found to be close to 0.95 as shown in Table 3.

The collection of MLEs is plotted in Fig. 9 while the lengths of the confidence intervals associated with the ML estimates are plotted in Fig. 10. Although the coverage for the cases when R_0 is before and after

the reinfection threshold were found to be comparable, we see that the lengths of the confidence interval have different distributions with R_0 values larger than the threshold having on average larger confidence intervals (Table 3). One possibility is that the narrower confidence intervals of the two smaller R_0 values are related to the oscillatory signal in the solutions in this case due to the complex eigenvalues of the endemic equilibrium Jacobian. The period of oscillations can be sensitive to parameter values [20] and this could improve identifiability of R_0 by preventing possible trade offs with reporting probability when fitting to data near endemic equilibrium (where reported prevalence levels can be computed from the equilibrium equations and the reporting probability) or trade off with other epidemiological parameters that affect transmission [21]. However, the period of the expected oscillations about the endemic equilibrium for parameter values chosen in Fig. 7(a)–(b) spans multiple years in both cases and is not easily observed in the one-year datasets that we generated. Thus, oscillations are probably not the reason for the smaller confidence intervals when working with relatively fast epidemics over short time periods. Rather, we see more clearly in Fig. 7(c)–(d) the sharp transition to larger prevalence of infections for R_0 values larger than the reinfection threshold, consistent with the results in Section 4. These higher prevalence values have visibly larger stochastic fluctuations in the simulations of reported cases. In addition, since larger R_0 values lead to larger transmission rates (β) which are multiplied by gamma-distributed white noise terms (with mean one and fixed intensity), the product yields a larger magnitude stochastic term that may be the reason for the wider confidence intervals that we measured. We also note that since all profiles were only computed from $R_0 = 1.5$ to $R_0 = 8$, the confidence intervals for some simulations may be artificially shortened in our measurements. This was more likely to happen in simulations with

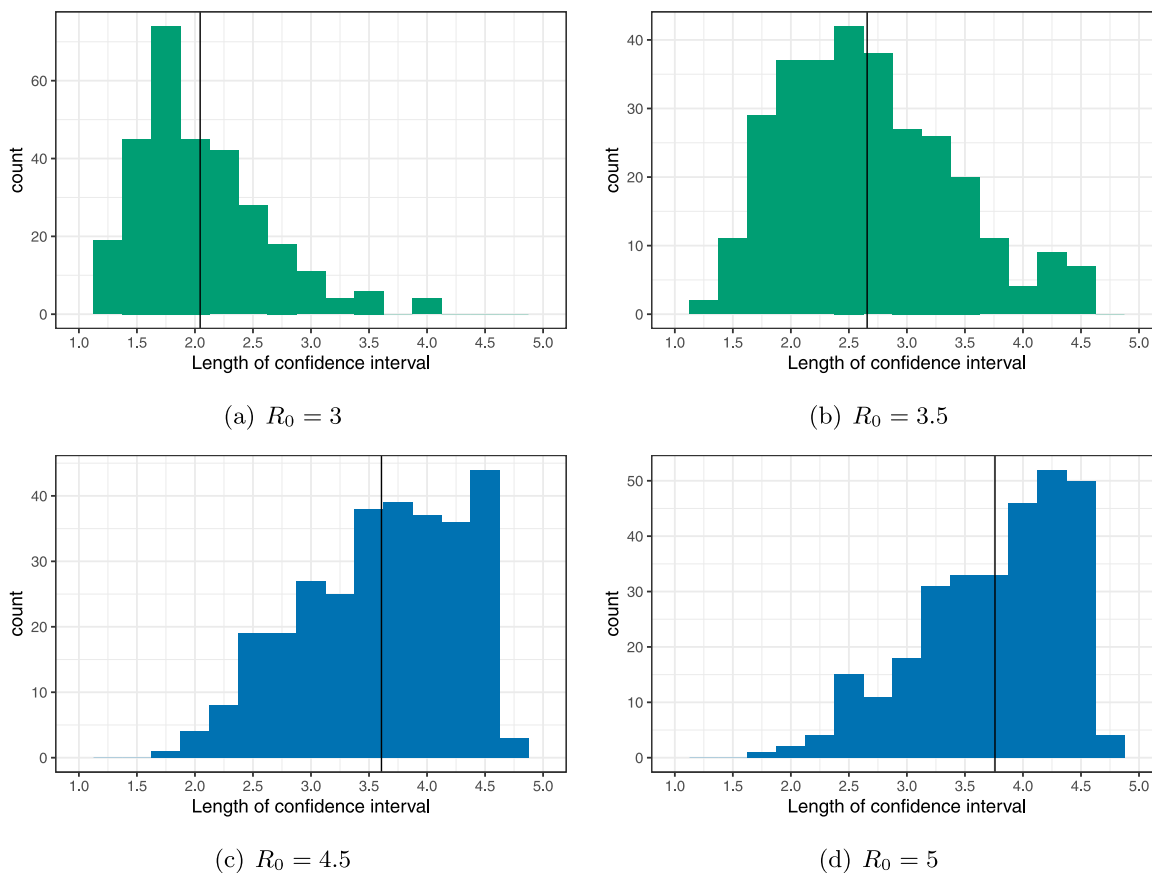


Fig. 10. Lengths of the 95% confidence intervals using profile likelihood for simulations generated with reproduction number values $R_0 < \frac{1}{\epsilon}$ for (a)–(b) and $R_0 > \frac{1}{\epsilon}$ for (c)–(d). The mean value of each distribution is denoted by vertical black lines. We see that the case $R_0 > \frac{1}{\epsilon}$ has larger confidence intervals.

larger R_0 values, and thus the true confidence interval length may actually be even larger for the larger R_0 values.

7. Conclusions and future work

One way the SIR and SIS models can be connected is via a continuous scale of leaky infection-derived immunity. Previous authors have noted differences in model behavior when parameter values are chosen on either side of a so-called reinfection threshold, which occurs when the basic reproduction number equals the inverse of the leakiness. While it has previously been shown that this threshold has some important implications regarding controllability when vaccination has the same leaky level of partial protection, a technical description of the qualitative change that occurs near the reinfection threshold for the model without vaccination was more difficult to derive. In this paper, we revisited the reinfection threshold and showed that it is related to two important events: First, for a fixed value of leakiness, the basic reproduction number value at which the endemic equilibrium changes from being a stable spiral (as in the SIR system for commonly used reasonable parameter values as discussed in Remark 3.4) back to a stable node (as in the SIS system) converges to the value given by the reinfection threshold in the limit as q approaches one. Second, for a fixed basic reproduction number value, the leakiness value at which the maximum rate of change of the prevalence occurs approaches its reinfection threshold value as q approaches one. For acute diseases wherein the recovery period is much shorter than the lifetime of an individual, it follows that the value of q is close to one. Thus our results are applicable to a wide range of diseases that we might want to model. We also showed how these conditions and results are related

to previous work by Stollenwerk et al. [10] and Martins et al. [11] on models with both leaky and waning infection-derived immunity.

Using a simulation study on a stochastic version of the model and the default parameter values in Table 1, we also found that estimates of R_0 are more precise when the true value of R_0 the value of R_0 used to generate the simulations is before the reinfection threshold. While this could be related to the oscillatory behavior of solutions before the threshold (as in Fig. 3(a)), this oscillatory behavior is not evident in the simulations of reported cases for R_0 values lower than the threshold (as shown in Fig. 7). Instead, we clearly see sharply higher prevalence values associated with R_0 values larger than its reinfection threshold value yielding noisier simulations of disease reporting data. It would be interesting to conduct further simulation studies to try to disentangle the effect of the reinfection threshold from that of simply larger R_0 values on parameter identifiability.

Our focus has been on the reinfection threshold associated with a simple disease transmission model with leaky infection-derived immunity. The same threshold value has been found to be important in other models [10–12]. It would be interesting to see if this same threshold concept applies to more complex models of immunity and what consequences of the threshold are maintained in those cases. Rapidly growing interest in the analysis and inference of disease models, spurred by the COVID-19 pandemic, suggests that further study of this phenomenon is warranted.

Declaration of competing interest

None.

Data availability

Data will be made available on request.

Acknowledgments

We are grateful to T. Day for the helpful discussions. We acknowledge the support of the Natural Sciences and Engineering Research Council of Canada (NSERC) Discovery Grant Program. FMGM and SZ also acknowledge the support of the Mathematics for Public Health network from the NSERC Emerging Infectious Diseases Modelling Initiative. This work was conducted in part while FMGM was an academic visitor at the University of Oxford.

Appendix A. Supplementary data

Supplementary material related to this article can be found online at <https://doi.org/10.1016/j.mbs.2023.109045>. Datasets and code used to generate the figures in Sections 6 are available at: <https://doi.org/10.5061/dryad.cc2fqz6c3>.

References

- [1] H. Hethcote, The mathematics of infectious diseases, *SIAM Rev.* 42 (4) (2000) 599–653.
- [2] S. Riley, N. Ferguson, Smallpox transmission and control: Spatial dynamics in great britain, *Proc. Natl. Acad. Sci.* 103 (33) (2006) 12637–12642.
- [3] H.W. Hethcote, in: S.A. Levin, T.G. Hallam, L.J. Gross (Eds.), *Three Basic Epidemiological Models*, Springer Berlin Heidelberg, Berlin, Heidelberg, 1989, pp. 119–144.
- [4] A. Le, A.A. King, F.M.G. Magpantay, A. Mesbahi, P. Rohani, The impact of infection-derived immunity on disease dynamics, *J. Math. Biol.* 83 (6–7) (2021).
- [5] O. Diekmann, J. Heesterbeek, J. Metz, On the definition and the computation of the basic reproduction ratio R_0 in models for infectious diseases in heterogeneous populations, *J. Math. Biol.* 28 (4) (1990).
- [6] P. van den Driessche, J. Watmough, Reproduction numbers and sub-threshold endemic equilibria for compartmental models of disease transmission, *Math. Biosci.* 180 (1–2) (2002) 29–48.
- [7] M. Gomes, L. White, G. Medley, Infection, reinfection, and vaccination under suboptimal immune protection: Epidemiological perspectives, *J. Theoret. Biol.* 228 (4) (2004) 539–549.
- [8] R. Breban, S. Blower, The reinfection threshold does not exist, *J. Theoret. Biol.* 235 (2) (2005) 151–152.
- [9] M. Gomes, L. White, G. Medley, The reinfection threshold, *J. Theoret. Biol.* 236 (1) (2005) 111–113.
- [10] N. Stollenwerk, S. van Noort, J. Martins, M. Aguiar, F. Hilker, A. Pinto, G. Gomes, A spatially stochastic epidemic model with partial immunization shows in mean field approximation the reinfection threshold, *J. Biol. Dyn.* 4 (6) (2010) 634–649, PMID: 22881209.
- [11] J. Martins, A. Pinto, N. Stollenwerk, The maximum curvature reinfection threshold, *Ecol. Complex.* 40 (2019) 100791.
- [12] R. Pagliara, B. Dey, N.E. Leonard, Bistability and resurgent epidemics in reinfection models, *IEEE Control Syst. Lett.* 2 (2) (2018) 290–295.
- [13] P. van den Driessche, J. Watmough, Further notes on the basic reproduction number, *Math. Epidemiol.* (2008) 159–178.
- [14] N. Kharazian, F. Magpantay, The honeymoon period after mass vaccination, *Math. Biosci. Eng.* 18 (1) (2021) 354–372.
- [15] M. Grobman, Homeomorphisms of systems of differential equations, *Dokl. Akad. Nauk SSSR* 128 (5) (1959) 880–881.
- [16] P. Hartman, A lemma in the theory of structural stability of differential equations, *Proc. Amer. Math. Soc.* 11 (4) (1960) 610–620.
- [17] A.A. King, E. Ionides, C. Martinez Bretó, S.P. Ellner, M.J. Ferrari, S. Funk, S.G. Johnson, B.E. Kendall, M. Lavine, D. Nguyen, E.B. O’Dea, D.C. Reuman, H. Wearing, S.N. Wood, *pomp*: Statistical inference for partially observed Markov processes, 2022, R package, version 4.5.
- [18] A.A. King, D. Nguyen, E.L. Ionides, Statistical inference for partially observed Markov processes via the R package *pomp*, *J. Stat. Softw.* 69 (12) (2016) 1–43.
- [19] Daihai He, Edward L. Ionides, Aaron A. King, Plug-and-play inference for disease dynamics: measles in large and small towns as a case study, *J. R. Soc. Interface* 7 (43) (2009).
- [20] H.J. Wearing, P. Rohani, Estimating the duration of pertussis immunity using epidemiological signatures, *PLOS Pathogens* 5 (10) (2009) 1–11.
- [21] M. Martinez-Bakker, *The Drivers of Acute Seasonal Infectious Diseases* (Ph.D. thesis), University of Michigan, 2015.